Molecular BioSystems

View Online
Dynamic Article Links

Cite this: *Mol. BioSyst.*, 2011, **7**, 2711–2719

www.rsc.org/molecularbiosystems

PAPER

Traditional Chinese medicine, a solution for reducing dual stroke risk factors at once?†

Kuan-Chung Chen,[a] Kai-Wei Chang,[a] Hsin-Yi Chen[b] and Calvin Yu-Chian Chen*[abcd]

Received 4th May 2011, Accepted 14th June 2011
DOI: 10.1039/c1mb05164d

Based on genome wide association studies (GWAS), the activities of phosphodiesterase 4D (PDE4D) and 5-Lipoxygenase activating protein (ALOX5AP) were suggested as two of the major factors involved in ischemic stroke risks. Uncontrolled PDE4D activities often lead to cAMP-induced stroke and cardiovascular diseases. Overexpression of ALOX5AP, on the other hand, had been shown to play a major role in inflammation pathway that could induce the development of atherosclerosis and stroke. To eliminate the risk factors that lead to stroke, we reported the identification and analysis of dual-targeting compounds that could reduce PDE4D and ALOX5AP activities from traditional Chinese medicine (TCM). We employed world's largest TCM database, TCM Database@Taiwan, for *in silico* drug identification. We also introduced machine learning predictive models, as well as pharmacophore model, for characterizing the drug-like candidates. Both myristic acid and pentadecanoic acid were identified. The follow-up analysis on molecular dynamics simulation further determined the major roles of the carboxyl group for forming stable molecular interactions. Intriguingly, the carboxyl group demonstrated different bonding patterns with PDE4D and ALOX5AP, through electrostatic interaction and hydrogen bonds, respectively. In addition, the large volume occupied by the ligand hydrophobic regions could achieve inhibition through occupying the vacant spaces in the binding site. These pharmacophores held true for both candidates against each protein targets. Hence, we proposed the presence of the carboxyl group and hydrophobic regions as potent dual targeting features that inhibit both PDE4D and ALOX5AP activities.

Introduction

The World Health Organization (WHO) recognized stroke and cerebrovascular diseases, which cause 5.71 million people death in 2004, as the second leading cause of death worldwide.[1] Moreover, strokes are not only life threatening, but can also lead to severe brain damage and disabilities.[2] A recent study from the Icelandic Decode group has identified 2 novel stroke-related genes, phosphodiesterase 4D (PDE4D) and 5-Lipoxygenase activating protein (ALOX5AP), by using a genome-wide association screen.[3,4] PDE4D is one of the cyclic nucleotide phosphodiesterases that plays an important role in cell metabolism by hydrolysis, which subsequently regulates the concentration of second messenger cyclic AMP (cAMP). Low cAMP concentration could lead to proliferation and migration of smooth muscle cells, which could result in the thickening of blood vessel walls and could confer risks in the development of atherosclerosis, which is associated with ischemic stroke.[5] On the other hand, ALOX5AP actively converts arachadonic acid to potent inflammatory factor, leukotriene A4, which is further hydrolyzed into leukotriene B4. Intriguingly, these leukotriene products from the ALOX5AP pathway were associated with the development of atherosclerosis, and have been reported to be involved in obstructive sleep apnoea and ischemic strokes.[6] Furthermore, leukotriene induced the leukocyte chemotaxis and inflammatory responses, which are key processes in stroke-associated atherosclerosis.[5]

To eliminate stroke-linked factors, we aimed to identify compounds that may reduce PDE4D and ALOX5AP activation through *in silico* drug discovery methods. Moreover, we focused on the stroke reducing potentials of traditional Chinese medicine (TCM). TCM is a well-known medical practice that has been used for thousands of years. Our past

[a] *Laboratory of Computational and Systems Biology, School of Chinese Medicine, China Medical University, Taichung, 40402, Taiwan*
[b] *Department of Bioinformatics, Asia University, Taichung, 41354, Taiwan*
[c] *Department of Systems Biology, Harvard Medical School, Boston, MA 02115, USA*
[d] *Computational and Systems Biology, Massachusetts Institute of Technology, Cambridge, MA 02139, USA. E-mail: ycc@mail.cmu.edu.tw, ycc929@MIT.EDU; Tel: +1-617-353-7123*
† Electronic supplementary information (ESI) available. See DOI: 10.1039/c1mb05164d

studies in drug discovery have identified potential therapeutic TCM compounds for a wide range of diseases, including anti-viral, anti-inflammatory, and anti-tumor agents.[7–13] Our previous report on the identification of PDE4D inhibitors has suggested some potential TCM inhibitors, as well as some key binding features in the PDE4D binding site.[14] Additionally, we have developed world's largest 3D small molecule TCM Database, TCM Database@Taiwan,[15] which further enhances the *in silico* drug discovery process. All compounds were tested through the ADMET for drug safety profiling.[16] Quantitative structure–activity relationship (QSAR) models and molecular dynamics (MD) simulations were employed to identify and characterize potent dual target inhibitors against PDE4D as well as ALOX5AP.

Materials and methods

Data collection

The crystal structures of PDE4D (PDB ID: 3G4G)[17] and ALOX5AP (PDB ID: 2Q7M)[18] were obtained from RCSB Protein Data Bank. For training QSAR models, structure and activity data of PDE4D inhibitors from Aspiotis' study[19] and ALOX5AP inhibitors from Stock's study[20] were obtained. For pharmacophore models, PDE4D ligands from three different studies,[19,21,22] and the ALOX5AP ligands from Stock's study[20] were employed. All TCM 3D small molecules from TCM Database@Taiwan[15] were obtained for screening. All compounds were tested by Lipinski's Rule of Five[23] and their ionization states were adjusted to physiological pH using Accelrys Discovery Studio 2.5 (DS 2.5).

Virtual screening and ADMET

The virtual screening step was performed by LigandFit module[24] of DS 2.5 with the CHARMm force field.[25] The cAMP binding site for PDE4D was defined by ligands, RS-25344, and the binding site for ALOX5AP was defined by the inhibitor MK-591. L-454560[26] and MK591 were treated as the control compounds with respect to their targets. The ADMET tests were evaluated by DS 2.5.

QSAR modeling

The non-linear SVM and the linear MLR machine learning algorithms were employed to construct QSAR models. SVM model was established using LibSVM.[27] MLR model was built using MATLAB modules.[28] The regression version of SMV (SVR)[29] was established using gridregression.py program in the libsvm-2.91 package.[27]

Training data for QSAR models were built separately for each receptor. For building inhibitor QSAR models for PDE4D and ALOX5AP, 17 PDE4D inhibitors from Aspiotis' study[19] and 30 ALOX5AP inhibitors from Stock's study [Stock, 2010 #19] were employed for training, respectively. Genetic function approximation (GFA)[30] module from DS2.5 was employed to identify representative molecular descriptors. The square correlation coefficient (R2) to pIC50 values was assessed to determine the accuracy of each model. The descriptors identified were NPlusO_Count, Num_H_Acceptors, and Jurs_PPSA_3 for PDE4D; and ES_Sum_dssC, Num_ExplicitHydrogen, Jurs_PPSA_3, Jurs_RASA, Jurs_TASA, Jurs_WNSA_3, JX for ALOX5AP. Five-fold cross validations were performed for both MLR and SVM models.

Pharmacophore modeling

62 PDE4D ligands[19,21,22] and 30 ALOX5AP ligands[20] were employed for building pharmacophore models. Molecules from the training sets were modified to low-energy conformations using FAST generation module in DS2.5. Common ligand features were identified by the HipHop algorithm.[31] HypoGen algorithm[32] then constructed the 3D-QSAR models based on the common pharmacophore features identified.

Molecular dynamics simulation

DS2.5 Simulation package was employed for MD simulation. A 7 Å radius solvation shell was created and ionically balanced for each simulation system. 6000 cycles of each Steepest Descent[33] with restricted protein and Conjugate Gradient[34] with flexible protein were performed for minimization. All hydrogen-linked bonds were fixed by the SHAKE algorithm. The long-range electrostatics was treated by the PME method. The simulation system was heated to 310 K in 50 ps intervals, followed by 200 ps of equilibration. For the production step, a constant temperature ensemble (NVT) with 0.4 ps of temperature coupling decay time was maintained. The time step was set to 0.002 ps throughout the simulation. MD simulation was performed for 22 ns.

Results and discussion

Screening and modeling

Virtual screening. Virtual screening identified 9 compounds that have higher Dock Scores[24] than both controls, L-454560 and MK-591 (Table 1). In addition, the ADMET test results suggested that all candidates could be carried by plasma proteins and could cause little interference in metabolism based on their probability of inhibiting cytochrome P450 (Table 1). Intriguingly, the absorption model suggested all candidates have good absorption probability (Fig. S1, ESI†).

Table 1 Docking results for the top TCM candidates and controls. The distribution and metabolism evaluation were included

Name	PPB[c] Level	CYP2D6[d] Probability	Dock score PDE4D	ALOX5AP	Total
Myristic acid	1	0.138	655.663	93.792	749.455
Pentadecanoic acid	1	0.386	652.648	91.21	743.858
2-pentadecenoic acid	1	0.386	646.995	90.1	737.095
2-hexadecenoic acid	1	0.386	644.702	90.28	734.982
9,12-Octadecadienoic acid	1	0.386	634.929	97.48	732.409
Hexadecanoic acid	1	0.386	640.171	90.234	730.405
11-hexadecenoic acid	1	0.386	640.956	86.888	727.844
Palmitoleic acid	1	0.386	638.934	87.454	726.388
Punicic acid	1	0.386	631.541	94.217	725.758
L-454560[a]	1	0.485	130.067	—	—
MK-591[b]	2	0.306	—	84.995	—

[a] Control for PDE4D. [b] Control for ALOX5AP. [c] Plasma Protein Binding: 1 = Binding > 90%; 2 = Binding > 95%. [d] Inhibition probability of Cytochrome P450 2D6 enzyme.

Comparatively, both controls were less likely to be absorbed through the human digestive system.

QSAR modeling. MLR and SVM prediction models were built based on the training data with 5-fold validation.

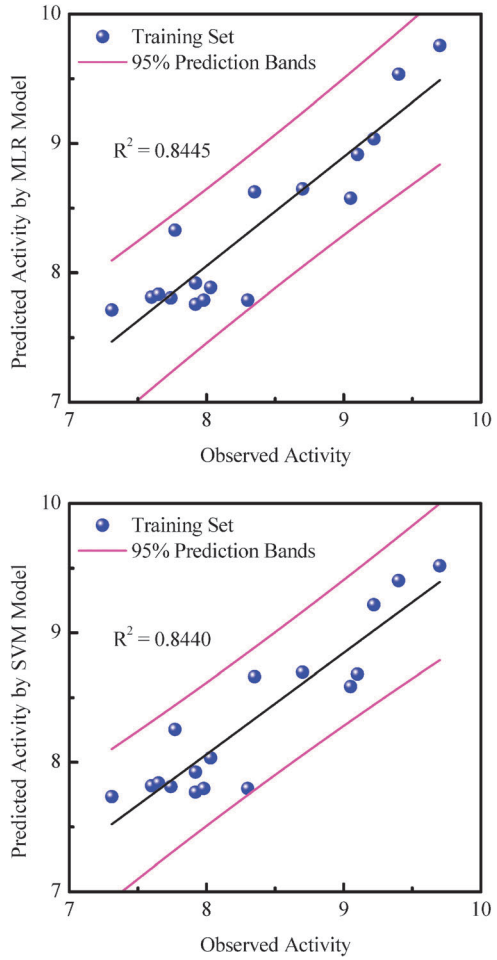

Fig. 1 Comparative plots of MLR (top) and SVM (bottom) models for PDE4D inhibitors. Correlation trend (black line) and 95% confidence regions (enclosed by magenta lines) were shown. Training set (blue dots) was presented.

Table 2 Predicted pIC50 for top TCM candidates and controls for each target protein

	PDE4D		ALOX5AP	
Name	MLR	SVM	MLR	SVM
Myristic acid	6.13	8.19	7.12	6.68
Pentadecanoic acid	6.16	8.19	7.87	6.46
2-pentadecenoic acid	6.26	8.16	8.35	6.55
2-hexadecenoic acid	6.27	8.16	8.63	6.47
9,12-Octadecadienoic acid	6.36	8.02	7.35	6.53
Hexadecanoic acid	6.26	8.20	8.38	6.64
11-hexadecenoic acid	6.36	8.24	8.08	6.81
Palmitoleic acid	6.17	8.22	7.29	6.70
Punicic acid	6.44	8.23	9.81	6.42
L-454560[a]	7.92	7.92	—	—
MK-591[b]	—	—	4.75	8.36

[a] Control for PDE4D. [b] Control for ALOX5AP.

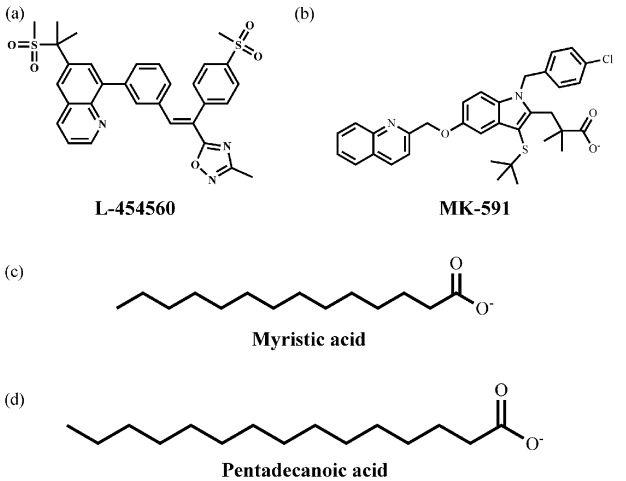

Fig. 2 The molecular structures of (a) L-454560, (b) MK-591, (c) Myristic acid, and (d) Pentadecanoic acid.

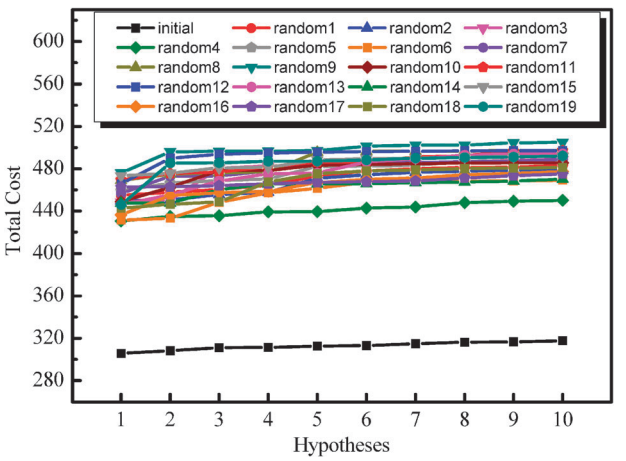

Fig. 3 CatScramble validation plot for PDE4D that compares total costs between the initial and randomized HypoGen hypothesis.

The R^2 of MLR and SVM models for PDE4D inhibitors were 0.8445 and 0.8440, respectively (Fig. 1). The same modeling process was applied for ALOX5AP, and the R^2 of MLR and SVM models were 0.7153 and 0.6589, respectively (Fig. S2, ESI†). The MLR prediction models with optimized property descriptors were described as the following:

PDE4D:

$$\text{predicted\_}pIC_{50} = 3.890 - 2.1921 \times \text{NPlusO\_Count} + 2.8165 \times \text{Num\_H\_Acceptors} + 0.0790 \times \text{Jurs\_PPSA\_3}$$

ALOX5AP:

$$\text{predicted\_}pIC_{50} = 43.786 + 3.2581 \times \text{ES\_Sum\_dssC} - 0.3154 \times \text{Num\_ExplicitHydrogen} - 0.1923 \times \text{Jurs\_PPSA\_3} - 78.1368 \times \text{Jurs\_RASA} + 0.0579 \times \text{Jurs\_TASA} + 0.0837 \times \text{Jurs\_WNSA\_3} + 6.4741 \times \text{JX}$$

The models were further validated by predicting the bioactivities of L-454560 and MK-591. The predicted pIC_{50} of L-454560 were 7.92 for both models, where the experimental IC_{50} was 1.2 nM,[26] which corresponds to a pIC_{50} of 8.92. With regard to MK-591, MLR and SVM showed diverse results of 4.75 and 8.36, respectively. Intriguingly, the experimental data

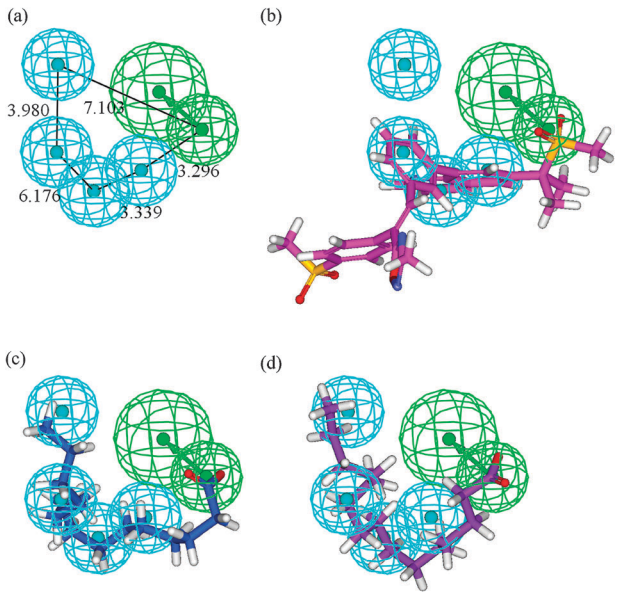

Fig. 4 HypoGen results of (a) pharmacophores map with labelled distances for PDE4D inhibitors, (b) mapping with L-454560, (c) mapping with Myristic acid, and (d) mapping with Pentadecanoic acid. The hydrophobic region (blue sphere), hydrogen bond acceptor region (green sphere) and hydrogen bond partner direction (green arrow) are presented.

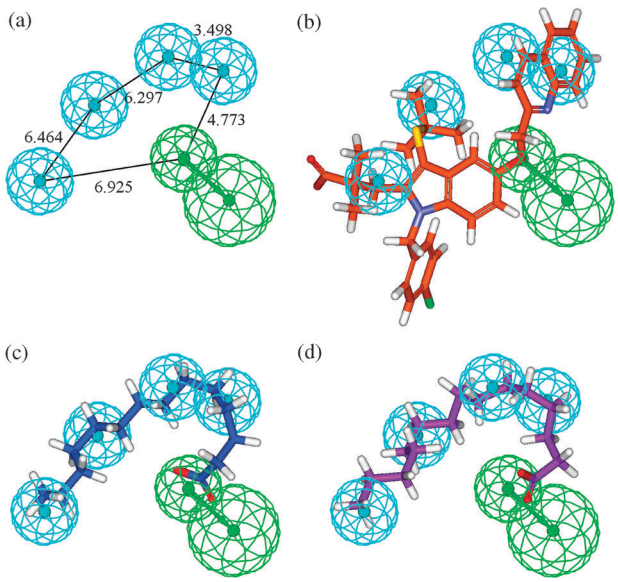

Fig. 5 HypoGen results of (a) pharmacophores map with labelled distances for ALOX5AP inhibitors, (b) mapping with MK-591, (c) mapping with Myristic acid, and (d) mapping with Pentadecanoic acid. The hydrophobic region (blue sphere), hydrogen bond acceptor region (green sphere) and hydrogen bond partner direction (green arrow) are presented.

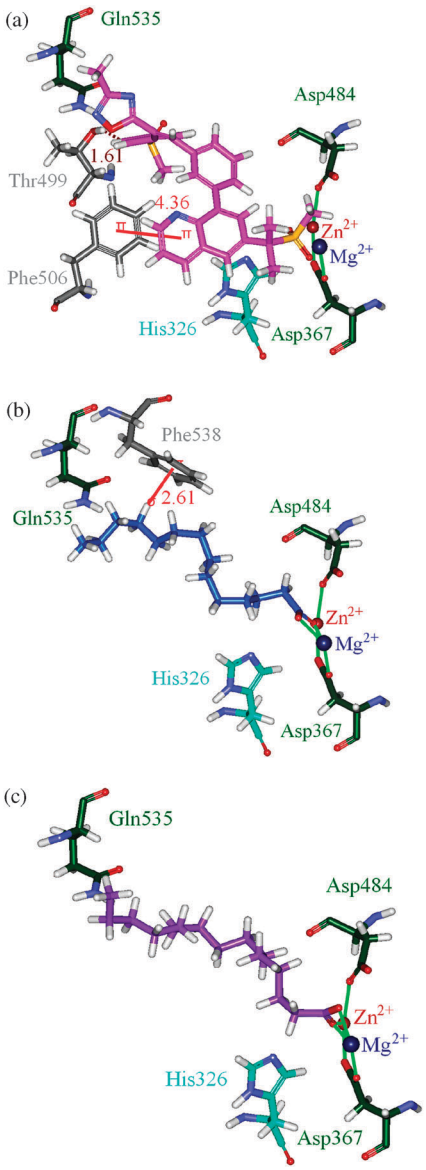

Fig. 6 Docking poses of PDE4D with (a) L-454560, (b) Myristic acid, and (c) Pentadecanoic acid in cAMP binding site. Residues of binding site (dark green), active site (cyan), and other residues (gray) were shown. Electrostatic interactions (green line), π–π interactions (red line) and hydrogen bond interactions (brown dashed line) are presented.

for MK-591 also showed a wide range of pIC_{50} values, including 8.80 (IC_{50} = 1.6 nM),[35,36] 8.70 (IC_{50} = 2.0 nM),[37–39] 8.64 (IC_{50} = 2.3 nM),[40] 6.70 (IC_{50} = 200 nM),[41] and 5.10 (IC_{50} = 8000 nM).[41] Hence, all bioactivity predictions for each inhibitor were within the acceptable range. Both models were employed to evaluate the compounds from screening results (Table 2). The predicted pIC_{50} for each candidates indicated that these candidates were potential dual target inhibitors for both PDE4D and ALOX5AP.

Pharmacophore models. In this study, we aimed to investigate the candidacies of the top two compounds, myristic acid (top1) and pentadecanoic acid (top2) based on the screening and QSAR modeling results. The structures of L-454560,

MK-591, and the top two common candidates, myristic acid and pentadecanoic acid, were shown in Fig. 2. We further built a HypoGen model for characterizing the pharmacophores based on the 3D structures of the candidates and the controls. The best pharmacophore hypothesis for each PDE4D and ALOX5AP has obtained over 190 and over 40 in cost difference, respectively (Table S1 and S2, ESI†). The results suggested the HypoGen models had more than 75% probability in representing a true correlation to the data. In addition, the *R* values for PDE4D and ALOX5AP pharmacophore models were 0.842 and 0.768, respectively. The CatScramble plots for PDE4D (Fig. 3) also implied the confidence of the HypoGen predictive models. Similarly, the ALOX5AP CatScramble plot suggested a representative HypoGen model (Fig. S3, ESI†). Final HypoGen models were hypothesized to have one hydrogen bond (H-bond) acceptor and 4 hydrophobic regions (Table S1 and S2, ESI†). By mapping each TCM candidate to the HypoGen models, the candidates and the controls showed satisfactory structures and features that matched with the given pharmacophore profiles (Fig. 4 and 5). The hydrophobic chains on the ligands mapped well with the hydrophobic regions defined by the models. In addition, carboxyl groups on candidates, as well as the oxygen atoms on the controls, mapped to the H-bond acceptor.

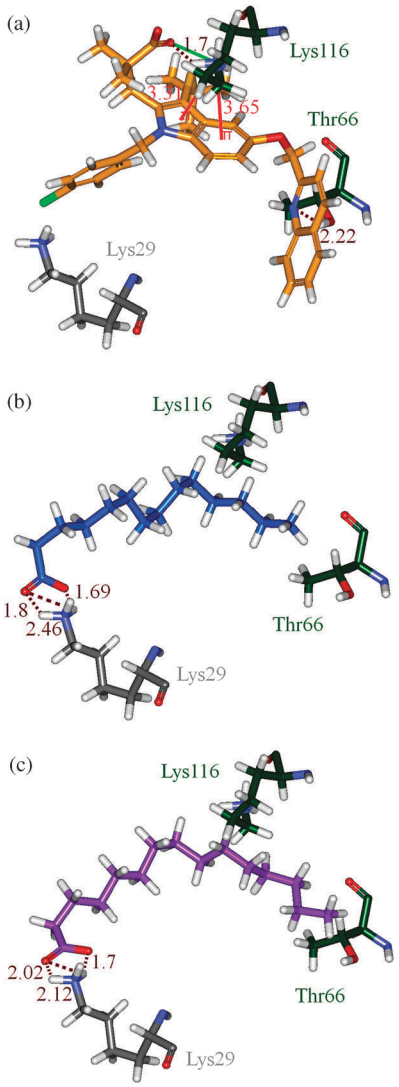

Fig. 7 Docking poses of ALOX5AP with (a) MK-591, (b) Myristic acid, and (c) Pentadecanoic acid. Residues for protein chain D (dark green) and protein chain E (gray) are shown. Electrostatic interactions (green line), π–cation interactions (red line) and hydrogen bond interactions (brown dashed line) are presented.

Docking conformations

Fig. 6 demonstrates the docking conformations of L-454560 and the top two TCM candidates. As shown in the figure, only L-454560 had one stabilizing H-bond, which interacted with Thr499. Additionally, the π–π interaction with Phe506 also

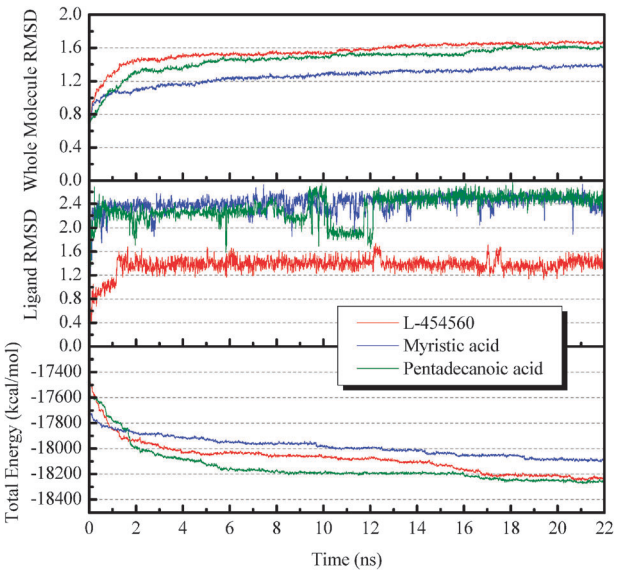

Fig. 8 MD dynamics trajectories of (a) whole molecule RMSD, (b) ligand RMSD, and (c) total energy of PDE4D in complex with each candidate and L-454560.

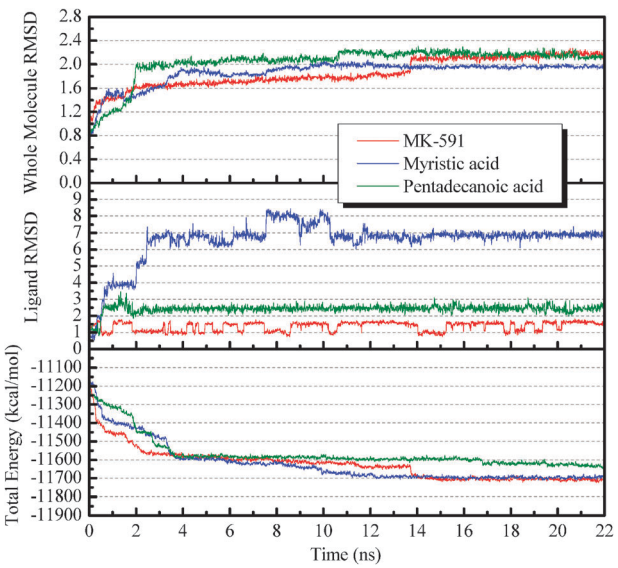

Fig. 9 MD dynamics trajectories of (a) whole molecule RMSD, (b) ligand RMSD, and (c) total energy of ALOX5AP in complex with each candidate and MK-591.

contributed to the binding affinity (Fig. 6a). On the other hand, the top two candidates had carboxyl groups that had electrostatic interactions with the two divalent metal cations, Zn^{2+} and Mg^{2+}, which mediated the binding to key residues, Asp367 and Asp484 (Fig. 6b and c).

Additionally, the aliphatic tail of each candidate was held at close approximation with the key residue Gln535, from which the binding function may be interfered. Fig. 7 shows the intermolecular interactions between ligands and ALOX5AP. The control MK-591 had high binding affinity to Lys116 with H-bond, pi–cation interaction, and electrostatic interaction on chain D, based on crystalized ALOX5AP structure. In addition, MK-591 also formed an H-bond Thr66 on Chain D that enhanced binding affinity. Comparatively, both candidates formed a stabilizing H-bond with Lys29 on chain E. Intriguingly, the aliphatic tail of each candidate reached to the key residues Lys116 as well as Thr66, and might inhibit the residues' activities.

Molecular dynamics simulation

MD simulation was employed to validate the binding stabilities of each protein–ligand interaction. The root mean square deviation (RMSD) trajectories were evaluated. We also keep track of the changes in the total energy of each binding pose during the simulation process. These trajectory data suggested

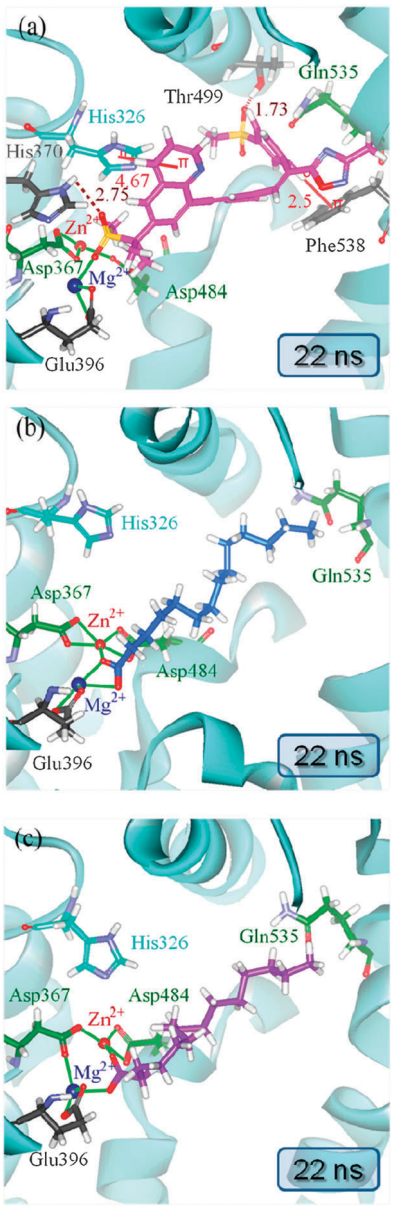

Fig. 10 The docking poses for PDE4D with (a) L-454560, (b) Myristic acid, and (c) Pentadecanoic acid at 22 ns of MD. Residues of binding site (dark green), active site (cyan), and other residues (gray) are shown. Electrostatic interactions (green line), π–π interactions (red line) and hydrogen bond interactions (brown dashed line) are presented.

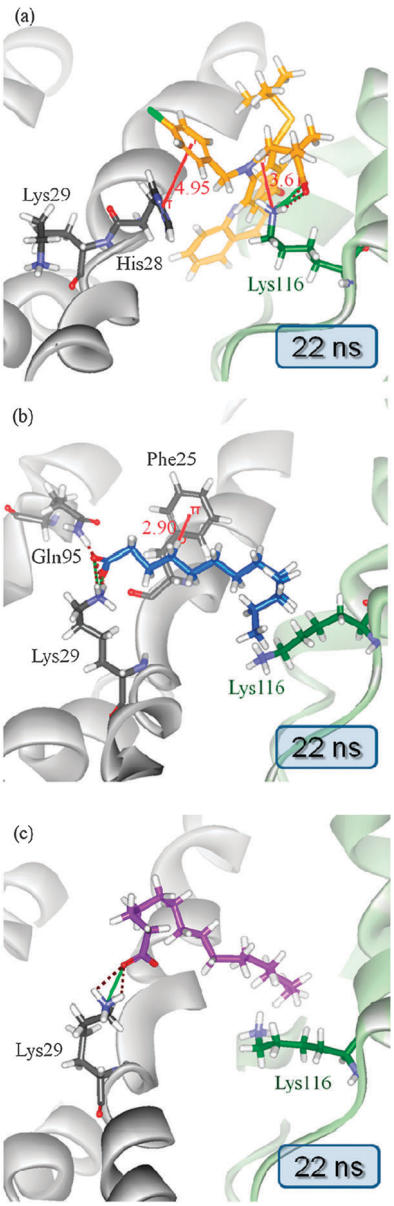

Fig. 11 The docking poses for ALOX5AP with (a) MK-591, (b) Myristic acid, and (c) Pentadecanoic acid at 22 ns of MD. Residues for protein chain D (dark green) and protein chain E (gray) are shown. Electrostatic interactions (green line), π–cation interactions (red line) and hydrogen bond interactions (brown dashed line) are presented.

that all PDE4D–ligand interactions (Fig. 8) and all ALOX5AP–ligand (Fig. 9) interactions stabilized after approximately 14 ns. Both L-454560 and MK-591 had ligand RMSDs of approximately 1.5 Å. However, MK-591 fluctuated between two RMSDs, which may imply alternative binding poses. The top1 candidate stabilized in PDE4D and ALOX5AP at ligand RMSD of 2.4 Å and 7 Å, respectively, and the top2 candidate stabilized at 2.4 Å ligand RMSD in both targets. Although all of the binding conformations stabilized relatively early, occasional fluctuations were observed in some trajectories. Intriguingly, the controls L-454560 and MK-591 showed more frequent fluctuation rates at ligand RMSD. In comparison, top1 and top2 ligands were relatively stable, with a fluctuation range of less than 1 Å.

Snapshots of each docking pose at 22 ns of simulation are presented in Fig. 10 for PDE4D and Fig. 11 for ALOX5AP. At the end of the MD simulation, L-454560 maintained tight cation-mediated (Zn^{2+} and Mg^{2+}) binding to Asp367 and ASP484 as well as the H-bond at Thr499 (Table 3 and Table S3, ESI†). Newly formed π-mediated bindings were

Table 3 H-bonds of PDE4D–ligand complexes for L-454560

Ligand	H-bond	Ligand atom	Amino acid	Max. distance	Average distance	Min. distance	H-bond occupancy[a]
L-454560	1	O22	His370:HD1	5.16	2.97	2.02	2.41%
	2	O40	Thr499:HG1	3.91	2.07	1.58	78.41%

[a] H-bond occupancy cutoff: 2.5 Å.

Table 4 H-bonds of ALOX5AP–ligand complexes for the top two candidates and MK-591

Ligand	H-bond	Ligand atom	Amino acid	Max. distance	Average distance	Min. distance	H-bond occupancy[a]
Myristic acid	1	O13	E:Lys29:HZ1	4.03	2.35	1.63	90.91%
	2	O14	E:Lys29:HZ1	5.10	2.73	1.73	71.50%
	3	O13	E:Lys29:HZ2	4.13	3.13	1.76	56.95%
	4	O14	E:Lys29:HZ2	5.35	3.80	1.63	14.09%
	5	O13	E:Lys29:HZ3	3.67	2.30	1.61	2.00%
	6	O14	E:Lys29:HZ3	4.96	3.29	1.68	76.86%
	7	O13	E:Gln95:HE22	7.66	3.23	2.48	12.23%
	8	O14	E:Gln95:HE22	5.69	2.36	1.85	0.05%
Pentadecanoic acid	1	O16	E:Lys29:HZ1	3.77	2.61	1.55	42.51%
	2	O17	E:Lys29:HZ1	5.23	4.03	1.85	0.68%
	3	O16	E:Lys29:HZ2	3.92	2.61	1.59	43.46%
	4	O17	E:Lys29:HZ2	5.39	4.00	1.76	0.36%
	5	O16	E:Lys29:HZ3	3.75	2.67	1.60	39.51%
	6	O17	E:Lys29:HZ3	5.31	4.07	1.82	0.59%
MK-591	1	O4	D:Lys116:HZ1	4.49	2.63	1.63	37.82%
	2	O5	D:Lys116:HZ1	3.81	2.52	1.62	48.50%
	3	O4	D:Lys116:HZ2	4.87	2.60	1.59	39.82%
	4	O5	D:Lys116:HZ2	3.92	2.53	1.61	50.45%
	5	O4	D:Lys116:HZ3	4.65	2.64	1.64	36.86%
	6	O5	D:Lys116:HZ3	3.93	2.57	1.63	45.32%

[a] H-bond occupancy cutoff: 2.5 Å.

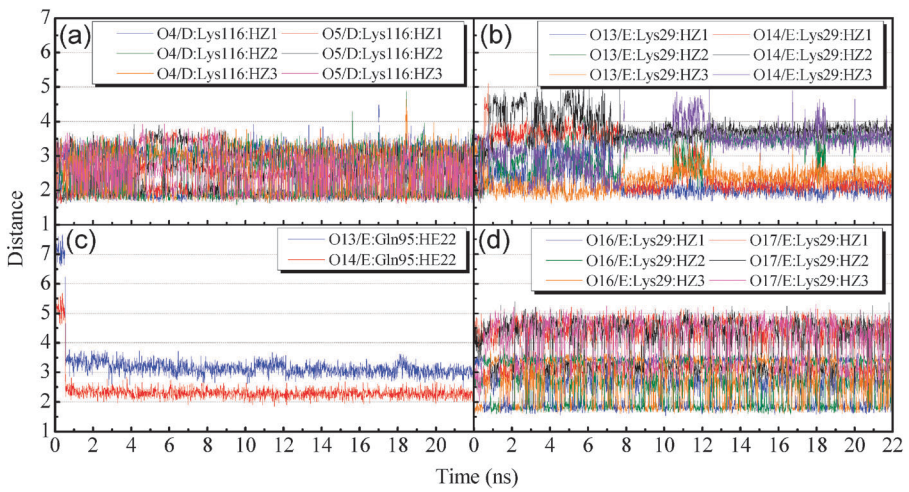

Fig. 12 Distance in Å of hydrogen bonds between ALOX5AP and (a) MK-591, (b)(c) Myristic acid, and (d) Pentadecanoic acid.

observed, including π–π interactions at His326 and π–sigma interactions at Phe538 (Fig. 10a). In addition, the binding poses showed that an additional H-bond was formed at His370, which supported the pharmacophore hypothesis at the H-bond acceptor region (Fig. 4b). With regard to the candidates, the carboxyl groups maintained stable electrostatic interactions with the abovementioned cations, which held the key residues Asp367 and Asp484 in close approximation. Throughout the simulation, the aliphatic tails of the candidates were maintained within the PDE4D ligand binding site, which interfere with the key residue Gln535 (Fig. 10b and c).

All ALOX5AP–ligand interactions maintained the binding stabilities through H-bonds (Table 4, Fig. 12). The control MK-591 was held at close approximation to Lys166 at chain D by H-bonds throughout the simulation (Fig. 12a). Based on the snapshots, a new π–π interaction was formed between MK-591 and His28 at chain E (Fig. 11a). For both candidates, the carboxyl groups presented in the snapshots maintained stable electrostatic interactions and H-bonds with Lys29 (Table 4, Fig. 11b and c). Moreover, the top1 candidate formed a new H-bond with Gln95 at chain E, as well as a new π–sigma interaction with Phe25, which further contributed to the protein–ligand binding stabilities.

Conclusion

Based on the analysis, the binding poses of both top1 and top2 candidates suggested common interaction patterns that fitted in both the PDE4D and ALOX5AP binding sites. As suggested by the screening results, TCM compounds that contained an acidic carboxyl group could lead to better target–ligand interactions. The pharmacophore models further hypothesized that the presence of an H-bond donor as well as the presence of high volumes of hydrophobic regions were the key features for a potent ligand. As demonstrated in the MD simulation, the carboxyl group showed particularly interesting features for binding to the targets PDE4D and ALOX5AP. For PDE4D, the carboxyl group in each candidate showed strong binding affinities to the divalent cations (Zn^{2+} and Mg^{2+}), which bridged the binding stability to the key residues Asp367 and ASP484. For ALOX5AP, the carboxyl group formed stabilizing H-bonds with the receptor. The potent interaction between the ligand carboxyl group and the binding site allowed the hydrophobic volume to both fill the binding site and subsequently block the access to the key residues. Hence, as the analysis on the TCM candidates suggested, the presence of the carboxyl group and high hydrophobic volume were the key features for a dual-targeting inhibitor against PDE4D and ALOX5AP, which the proteins had critical roles as stroke risk factors.

Acknowledgements

The research was supported by grants from the National Science Council of Taiwan (NSC 99-2221-E-039-013-), Committee on Chinese Medicine and Pharmacy (CCMP100-RD-030), China Medical University and Asia University (CMU98-TCM, CMU99-TCM, CMU99-S-02, CMU99-ASIA-25, CMU99-ASIA-26 CMU99-ASIA-27 CMU99-ASIA-28). This study is also supported in part by the Taiwan Department of Health Clinical Trial and Research Center of Excellence (DOH100-TD-B-111-004) and Taiwan Department of Health Cancer Research Center of Excellence (DOH100-TD-C-111-005). We are grateful to the Asia University cloud-computing facilities.

References

1 World Health Organization, 2008.
2 M. N. Beckley, *Am. J. Occup. Ther.*, 2006, **60**, 129–135.
3 H. S. Markus and M. J. Alberts, *Stroke*, 2006, **37**, 288–290.
4 H. Lovkvist, J. G. Smith, H. Luthman, P. Hoglund, B. Norrving, U. Kristoffersson, A. C. Jonsson and A. G. Lindgren, *Eur. J. Hum. Genet.*, 2008, **16**, 1117–1125.
5 S. Gretarsdottir, G. Thorleifsson, S. T. Reynisdottir, A. Manolescu, S. Jonsdottir, T. Jonsdottir, T. Gudmundsdottir, S. M. Bjarnadottir, O. B. Einarsson, H. M. Gudjonsdottir, M. Hawkins, G. Gudmundsson, H. Gudmundsdottir, H. Andrason, A. S. Gudmundsdottir, M. Sigurdardottir, T. T. Chou, J. Nahmias, S. Goss, S. Sveinbjornsdottir, E. M. Valdimarsson, F. Jakobsson, U. Agnarsson, V. Gudnason, G. Thorgeirsson, J. Fingerle, M. Gurney, D. Gudbjartsson, M. L. Frigge, A. Kong, K. Stefansson and J. R. Gulcher, *Nat. Genet.*, 2003, **35**, 131–138.
6 B. Lefebvre, J. L. Pepin, J. P. Baguet, R. Tamisier, M. Roustit, K. Riedweg, G. Bessard, P. Levy and F. Stanke-Labesque, *The European respiratory journal: official journal of the European Society for Clinical Respiratory Physiology*, 2008, **32**, 113–120.
7 T. T. Chang, H. J. Huang, K. J. Lee, H. W. Yu, H. Y. Chen, F. J. Tsai, M. F. Sun and C. Y. C. Chen, *J. Biomol. Struct. Dyn.*, 2010, **28**, 309–321.
8 H. J. Huang, K. J. Lee, H. W. Yu, H. Y. Chen, F. J. Tsai and C. Y. C. Chen, *J. Biomol. Struct. Dyn.*, 2010, **28**, 187–200.
9 H. J. Huang, K. J. Lee, H. W. Yu, C. Y. Chen, C. H. Hsu, H. Y. Chen, F. J. Tsai and C. Y. C. Chen, *J. Biomol. Struct. Dyn.*, 2010, **28**, 23–37.
10 C. Y. Chen and C. Y. C. Chen, *J. Mol. Graphics Modell.*, 2010, **29**, 21–31.
11 C. Y. C. Chen, *J. Biomol. Struct. Dyn.*, 2010, **27**, 627–640.
12 C. Y. C. Chen, *J. Taiwan Inst. Chem. Eng.*, 2010, **41**, 143–149.
13 C. Y. C. Chen, *J. Mol. Graphics Modell.*, 2009, **28**, 261–269.
14 C. Y.-C. C. Kuan-Chung Chen, *Soft Matter*, 2011, **7**, 4001–4008.
15 C. Y.-C. Chen, *PLoS One*, 2011, **6**, e15939.
16 H. van de Waterbeemd and E. Gifford, *Nat. Rev. Drug Discovery*, 2003, **2**, 192–204.
17 A. B. Burgin, O. T. Magnusson, J. Singh, P. Witte, B. L. Staker, J. M. Bjornsson, M. Thorsteinsdottir, S. Hrafnsdottir, T. Hagen, A. S. Kiselyov, L. J. Stewart and M. E. Gurney, *Nat. Biotechnol.*, 2010, **28**, 63–70.
18 A. D. Ferguson, B. M. McKeever, S. Xu, D. Wisniewski, D. K. Miller, T. T. Yamin, R. H. Spencer, L. Chu, F. Ujjainwalla, B. R. Cunningham, J. F. Evans and J. W. Becker, *Science*, 2007, **317**, 510–512.
19 R. Aspiotis, D. Deschenes, D. Dube, Y. Girard, Z. Huang, F. Laliberte, S. Liu, R. Papp, D. W. Nicholson and R. N. Young, *Bioorg. Med. Chem. Lett.*, 2010, **20**, 5502–5505.
20 N. Stock, C. Baccei, G. Bain, A. Broadhead, C. Chapman, J. Darlington, C. King, C. Lee, Y. W. Li, D. S. Lorrain, P. Prodanovich, H. J. Rong, A. Santini, J. Zunic, J. F. Evans, J. H. Hutchinson and P. Prasit, *Bioorg. Med. Chem. Lett.*, 2010, **20**, 213–217.
21 G. L. Card, L. Blasdel, B. P. England, C. Zhang, Y. Suzuki, S. Gillette, D. Fong, P. N. Ibrahim, D. R. Artis, G. Bollag, M. V. Milburn, S. H. Kim, J. Schlessinger and K. Y. Zhang, *Nat. Biotechnol.*, 2005, **23**, 201–207.
22 K. Naganuma, A. Omura, N. Maekawara, M. Saitoh, N. Ohkawa, T. Kubota, H. Nagumo, T. Kodama, M. Takemura, Y. Ohtsuka, J. Nakamura, R. Tsujita, K. Kawasaki, H. Yokoi and M. Kawanishi, *Bioorg. Med. Chem. Lett.*, 2009, **19**, 3174–3176.
23 C. A. Lipinski, F. Lombardo, B. W. Dominy and P. J. Feeney, *Adv. Drug Delivery Rev.*, 2001, **46**, 3–26.
24 C. M. Venkatachalam, X. Jiang, T. Oldfield and M. Waldman, *J. Mol. Graphics Modell.*, 2003, **21**, 289–307.

25 B. R. Brooks, C. L. Brooks, A. D. Mackerell, L. Nilsson, R. J. Petrella, B. Roux, Y. Won, G. Archontis, C. Bartels, S. Boresch, A. Caflisch, L. Caves, Q. Cui, A. R. Dinner, M. Feig, S. Fischer, J. Gao, M. Hodoscek, W. Im, K. Kuczera, T. Lazaridis, J. Ma, V. Ovchinnikov, E. Paci, R. W. Pastor, C. B. Post, J. Z. Pu, M. Schaefer, B. Tidor, R. M. Venable, H. L. Woodcock, X. Wu, W. Yang, D. M. York and M. Karplus, *J. Comput. Chem.*, 2009, **30**, 1545–1614.
26 D. Macdonald, A. Mastracchio, H. Perrier, D. Dube, M. Gallant, P. Lacombe, D. Deschenes, B. Roy, J. Scheigetz, K. Bateman, C. Li, L. A. Trimble, S. Day, N. Chauret, D. A. Nicoll-Griffith, J. M. Silva, Z. Huang, F. Laliberte, S. Liu, D. Ethier, D. Pon, E. Muise, L. Boulet, C. C. Chan, A. Styhler, S. Charleson, J. Mancini, P. Masson, D. Claveau, D. Nicholson, M. Turner, R. N. Young and Y. Girard, *Bioorg. Med. Chem. Lett.*, 2005, **15**, 5241–5246.
27 R. E. Fan, P. H. Chen and C. J. Lin, *J. Mach. Learn. Res.*, 2005, **6**, 1889–1918.
28 A. K. Saxena and P. Prathipati, *SAR QSAR Environ. Res.*, 2003, **14**, 433–445.
29 A. J. Smola and B. Scholkopf, *Stat. Comput.*, 2004, **14**, 199–222.
30 D. Rogers and A. J. Hopfinger, *J. Chem. Inf. Comput. Sci.*, 1994, **34**, 854–866.
31 A. T. M. O. O. Clement, in *Pharmacophore Perception, Development, and Use in Drug Design*, ed. O. F. Güner, International University Line, La Jolla, CA, 2000, ch. 69–84.
32 J. S. a. R. H. H. Li, in *Pharmacophore Perception, Development, and Use in Drug Design*, ed. O. F. Güner, International University Line, La Jolla, CA, 2000, pp. 171–189.
33 R. Fletcher, Academic Press, New York and London, 1969.
34 R. Fletcher and C. M. Reeves, *Comput. J.*, 1964, **7**, 149–154.
35 J. H. Hutchinson, S. Charleson, J. F. Evans, J. P. Falgueyret, K. Hoogsteen, T. R. Jones, S. Kargman, D. Macdonald, C. S. McFarlane and D. W. Nicholson, *et al.*, *J. Med. Chem.*, 1995, **38**, 4538–4547.
36 D. Macdonald, C. Brideau, C. C. Chan, J. P. Falgueyret, R. Frenette, J. Guay, J. H. Hutchinson, H. Perrier, P. Prasit, D. Riendeau, P. Tagari, M. Therien, R. N. Young and Y. Girard, *Bioorg. Med. Chem. Lett.*, 2008, **18**, 2023–2027.
37 J. H. Hutchinson, Y. Li, J. M. Arruda, C. Baccei, G. Bain, C. Chapman, L. Correa, J. Darlington, C. D. King, C. Lee, D. Lorrain, P. Prodanovich, H. Rong, A. Santini, N. Stock, P. Prasit and J. F. Evans, *J. Med. Chem.*, 2009, **52**, 5803–5815.
38 R. Frenette, J. H. Hutchinson, S. Leger, M. Therien, C. Brideau, C. C. Chan, S. Charleson, D. Ethier, J. Guay, T. R. Jones, M. McAuliffe, H. Piechuta, D. Riendeau, P. Tagari and Y. Girard, *Bioorg. Med. Chem. Lett.*, 1999, **9**, 2391–2396.
39 P. Prasir, M. Belleya, C. Brideaua, C. Chana, S. Charlesona, J. F. Evansa, R. Fortina, A. W. Ford-Hutchinsona, J. W. Gillarda, J. Guaya, J. H. Hutchinsona, S. Légera, D. Riendeaua, R. N. Younga and R. Zambonia, *Bioorg. Med. Chem. Lett.*, 1992, **2**, 1395–1398.
40 J. H. Hutchinson, P. Prasita, L. Y. Choob, D. Riendeaub, S. Charlesonc, J. F. Evansc, H. Piechutac and R. G. Balld, *Bioorg. Med. Chem. Lett.*, 1992, **2**, 1699–1702.
41 K. W. Woods, C. D. W. Brooks, R. G. Maki, K. E. Rodriques, J. B. Bouska, P. Young, R. L. Bell and G. W. Carter, *Bioorg. Med. Chem. Lett.*, 1996, **6**, 1547–1552.